SynBio

MDPI

Article

Targeting Amphotericin B Delivery to Yeast with ApoA1 Lipid Nanodiscs Coupled to Dectin-1 Using a Modular SpyCatcher–SpyTag System

James A. Davis [1,†], Jaeden B. Tedsen [1,†], Elizabeth Brown [1], Luis Corona-Elizarraras [2], Gretchen Berg [1], Mario A. Alpuche-Aviles [2] and Jeffrey F. Harper [1,*]

[1] Department of Biochemistry and Molecular Biology, University of Nevada, Reno, Reno, NV 89557, USA; jamesd@unr.edu (J.A.D.)
[2] Department of Chemistry, University of Nevada, Reno, Reno, NV 89557, USA
* Correspondence: jfharper@unr.edu
† These authors contributed equally to this work.

Abstract

Lipid nanodiscs are synthetic nanoparticles capable of solubilizing lipophilic drugs and have been shown to improve the potency of the antifungal Amphotericin B (AmphB) against various fungal pathogens. In this study, the SpyCatcher–SpyTag covalent labeling system was used to couple AmphB-loaded Apolipoprotein A1 (ApoA1) lipid nanodiscs to the receptor domain of Dectin-1, which binds to β-1,3/1,6 glucans present in many fungal cell walls. Denaturing protein gel electrophoresis demonstrated that ApoA1-SpyTag003 lipid nanodiscs could be covalently labeled with SpyCatcher003-Dectin-1-superfolder GFP (sfGFP). In microtiter growth assays with *Saccharomyces cerevisiae*, Dectin-1 AmphB nanodiscs displayed an IC_{50} 1.5-fold lower than uncoupled AmphB nanodiscs and 2.8-fold lower than AmphB-only controls. Nanodiscs without AmphB and SpyCatcher003-Dectin-1-sfGFP themselves did not inhibit yeast growth. Fluorescence microscopy showed that SpyCatcher003-Dectin-1-sfGFP binds to yeast cell walls and accumulated at hot spots, matching the budding scar enrichment pattern previously described for other Dectin-1 fusion proteins. Together these results indicate that Dectin-1 fusions can target AmphB-loaded lipid nanodiscs to fungal cell walls and improve drug delivery. The results here establish the use of a modular SpyCatcher–SpyTag coupling system for targeting drug-loaded lipid nanodiscs to different cells or tissues, thereby increasing drug retention at infection sites, increasing drug potency, and reducing harmful side-effects.

Keywords: nanodiscs; SpyCatcher system; antifungal delivery

Check for updates

Academic Editor: Bernd Rehm

Received: 25 February 2026
Revised: 2 April 2026
Accepted: 8 April 2026
Published: 10 April 2026

Copyright: © 2026 by the authors. Licensee MDPI, Basel, Switzerland. This article is an open access article distributed under the terms and conditions of the Creative Commons Attribution (CC BY) license.

1. Introduction

Protein–lipid nanodiscs are synthetic nanoparticles composed of a hydrophilic protein ring with a core populated by membrane lipids [1,2]. Of the many proteins that can mediate the formation of lipid–protein nanostructures, amphipathic membrane scaffolding proteins like Apolipoproteins have garnered persistent interest. N-terminal truncations of Apolipophorin-III from insects and Apolipoprotein A and E variants from humans (e.g., ApoA1, ApoE3, etc.) readily form into nanodisc structures when sonicated in the presence of membrane lipids [3–6]. When sonicated in the presence of lipophilic drugs like antifungal Amphotericin B (AmphB), nanodiscs incorporate the drug into the hydrophobic lipid core [7,8]. Growth inhibition assays with various yeast species [8,9] and

plant pathogens [10] indicate that AmphB nanodiscs display superior efficacy in inhibiting fungal growth relative to an equivalent dose of AmphB alone or in deoxycholate or liposomal formulations.

To further improve the ability of nanodiscs to preferentially deliver hydrophobic drugs to specific destinations, a modular design strategy was devised to use the SpyCatcher–SpyTag covalent labeling system [11,12] to couple proteins that will direct and localize AmphB-loaded nanodiscs to fungal cell walls. In mammals, the extracellular domain of Dectin-1 is known to bind β-1,3/1,6 glucans present in many fungal cell walls [13,14]. After binding fungal β-glucans, Dectin-1 triggers Syk/CARD9 and Raf1 signaling pathways to promote inflammatory cytokine production, drive phagocytosis, and coordinate T-cell differentiation for adaptive immunity [15–18]. The extracellular β-glucan binding domain of Dectin-1 was previously used to "coat" liposomes containing AmphB, which increased efficacy in inhibiting *A. fumigatus* growth [19]. In this study, AmphB-loaded ApoA1-SpyTag003 nanodiscs were covalently coupled with SpyCatcher003-Dectin-1-superfolder GFP (sfGFP) and assessed for their impact on *S. cerevisiae* growth.

Here, we show that a modular SpyCatcher–SpyTag system can be used to label human ApoA1 nanodiscs with the mouse Dectin-1 receptor domain and can thereby increase the toxicity of AmphB nanodiscs in yeast growth assays. Dectin-1 AmphB nanodiscs displayed a half-maximal inhibitory concentration (IC_{50}) of 0.13 μg/mL, which was 1.5-fold lower than the same nanodiscs without an attached Dectin-1. Fluorescence microscopy showed that SpyCatcher003-Dectin-1-sfGFP stained the cell wall of *S. cerevisiae*, enriched primarily at budding scars. Together these results demonstrate a proof-of-concept technology whereby a lipophilic drug loaded into a lipid nanodisc can be directed and localized to a cellular target by coupling the nanodisc to a ligand-binding protein. The SpyCatcher system used here provides a flexible modular design that could be expanded to target the unique extracellular surface features of not only fungi but also bacteria or cancer cells.

2. Results

E. coli protein expression and 6xHis purification techniques were used to generate two protein modules, ApoA1-SpyTag003 and SpyCatcher003-Dectin-1-sfGFP (Figure 1). AmphB-loaded lipid nanodiscs were made with ApoA1-SpyTag003 protein, which was then split into two fractions, one kept as an unmodified control and a second used in a coupling reaction with SpyCatcher003-Dectin-1-sfGFP. Absorbance spectroscopy determined that >99.9% of the AmphB had been integrated into soluble lipid nanodiscs (Supplemental Figure S1). Sodium dodecyl sulfate polyacrylamide gel electrophoresis (SDS-PAGE) confirmed that the Dectin-1-labeled nanodiscs had formed covalent isopeptide linkages between the ApoA1 and Dectin-1-sfGFP fragments (Figure 1). An analysis of SDS-PAGE gel images indicated that the 35 kDa ApoA1-SpyTag003 protein was the limiting component and that it was no longer detectable after a coupling reaction with an approximate 1.5-fold excess of SpyCatcher003-Dectin-1-sfGFP (Supplemental Figure S2). This indicates that the coupling reaction had gone to completion in labeling all nanodiscs with Dectin-1.

Dectin-1 AmphB nanodisc size distribution was analyzed using dynamic light scattering, a technique that measures the hydrodynamic radius of nanoscale particles. Using this strategy, it was determined that 99.1% of the Dectin-1 AmphB nanodisc particles displayed a diameter size range of 20–38 nm, with a histogram center of 24 nm (Supplemental Figure S3). Trace amounts of larger nanoparticle sizes were also detected, perhaps indicative of some aggregation complexes.

Microtiter yeast growth assays were performed that compared AmphB nanodiscs, Dectin-1 AmphB nanodiscs, and AmphB-only controls. Growth was monitored over time by measuring the absorbance at OD600 for doses ranging from 0 to 1.2 μg/mL AmphB.

Comparisons of log-phase growth slopes (m) were used to calculate percent inhibition and ultimately IC_{50} values. Under our assay conditions, an IC_{50} of 0.36 µg/mL AmphB was measured for drug-only controls (Figure 2). Delivering AmphB packaged into ApoA1 lipid nanodiscs resulted in an IC_{50} of 0.2 µg/mL, a 1.8-fold reduction relative to AmphB-only controls. Dectin-1 AmphB nanodiscs displayed the lowest IC_{50} at 0.13 µg/mL, which was 1.5-fold lower than the AmphB nanodisc comparisons. This indicates that the Dectin-1 labeling improved the potency or delivery of AmphB nanodiscs to yeast cells.

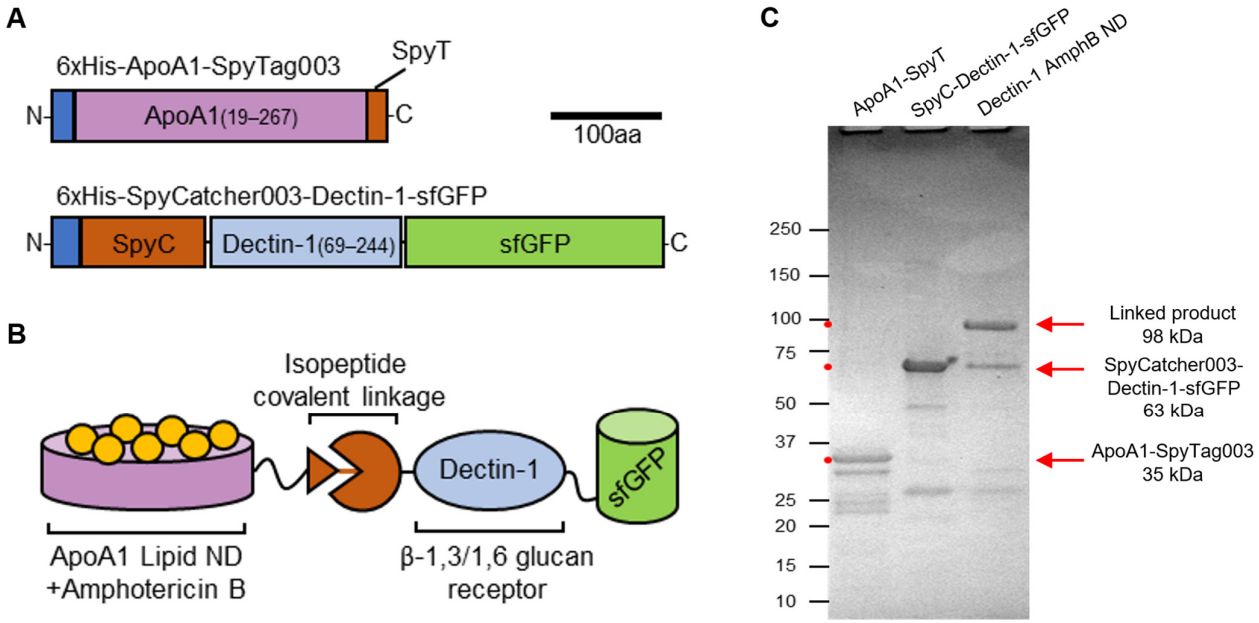


Figure 1. Protein gel analysis showing Dectin-1 labeling of lipid nanodiscs with SpyCatcher–SpyTag system. (**A**) Diagrams of 6xHis-ApoA1-SpyTag003 and 6xHis-SpyCatcher003-Dectin-1-sfGFP proteins used in this study. Elements are color coded: N-terminal 6xHis regions are dark blue, SpyCatcher (SpyC) and SpyTag (SpyT) are orange, ApoA1 is purple, Dectin-1 is light blue, and sfGFP is green. Encoded residues of human ApoA1 and mouse Dectin-1 are indicated. Proteins were expressed in *E. coli* and purified by 6xHis tags. (**B**) Depiction of a Dectin-1-labeled lipid nanodisc (ND) loaded with AmphB (gold balls). (**C**) SDS-PAGE analysis of 6xHis-ApoA1-SpyT, 6xHis-SpyC-Dectin-1-sfGFP, and Dectin-1 AmphB NDs. Protein ladder positions are indicated, and MW is provided in kDa. Red arrows and dots mark the bands of interest.

Similar yeast growth assays were performed as a control to determine whether equivalent concentrations of ApoA1-SpyTag003 nanodiscs lacking AmphB or SpyCatcher003-Dectin-1-sfGFP themselves were toxic to yeast. Dosages tested spanned the same concentrations of ApoA1 and Dectin-1 present in the Dectin-1 AmphB nanodisc samples. Under these concentrations, the ApoA1 nanodiscs and SpyCatcher003-Dectin-1-sfGFP controls failed to show any inhibition of yeast growth for all but the highest dose of Dectin-1 (Figure 3). A slight 17% growth inhibition was detected at 3.2 µg/mL SpyCatcher003-Dectin-1-sfGFP, but this corresponded to a dose 5-fold higher than the IC_{50} of Dectin-1 AmphB nanodiscs. Thus, any slight growth impact that free Dectin-1 can exert at high concentrations cannot explain the improved drug potency of Dectin-1 AmphB nanodiscs measured here.

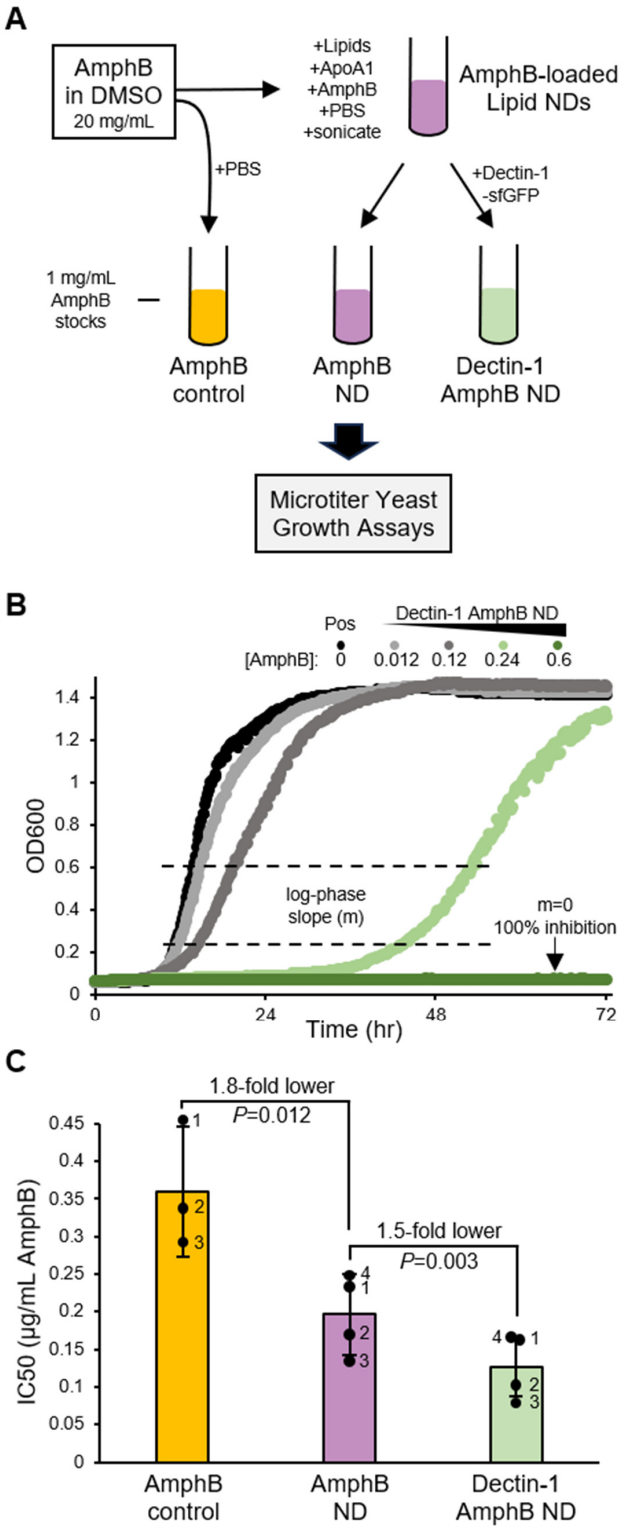


Figure 2. Growth assays showing that Dectin-1 labeling of AmphB nanodiscs improves efficacy in yeast growth inhibition. (**A**) Flow chart of lipid nanodisc (ND) formation and Dectin-1 labeling going into microtiter yeast growth assays. (**B**) Representative *S. cerevisiae* growth curves for Dectin-1 AmphB nanodiscs. [AmphB] provided in µg/mL. Data represent mean of n = 10 assay replicates. Percent inhibition was calculated from changes to log-phase growth slopes (% Inhibition = $(1 - (m/m_{pos})) \times 100\%$). Positive control (Pos) is no drug applied. (**C**) IC_{50} values generated from dose–response growth assays. Data represent mean ± STDEV. Each individual trial result is indicated by a black dot and numbered. n = 3–4 independent yeast growth assays and nanodisc preparations, with each assay containing 10 microtiter well technical replicates per treatment. p-values were calculated from paired Student's t-tests.

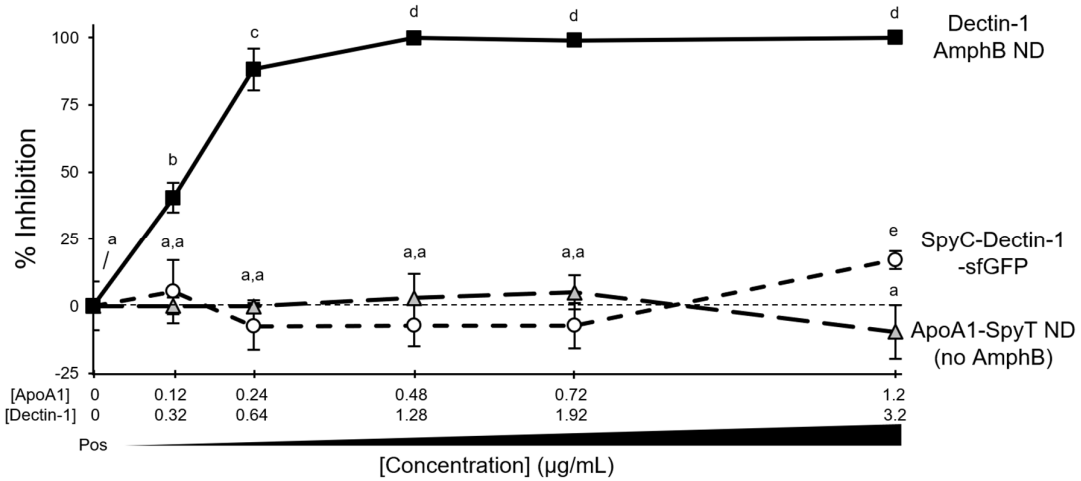


Figure 3. Growth inhibition analyses showing that ApoA1 nanodiscs and Dectin-1-sfGFP do not impact yeast growth. Percent growth inhibition for ApoA1-SpyT nanodiscs lacking AmphB (gray triangles) and SpyC-Dectin-1-sfGFP controls (white circles) relative to Dectin-1 AmphB nanodiscs (black squares). ApoA1-SpyT and SpyC-Dectin-1-sfGFP concentrations present in their respective experiments are provided in µg/mL. Data represent mean ± STDEV. n = 10 growth replicates and % inhibition calculations per condition. Different letters indicate significant differences from Tukey–Kramer HSD ($p < 0.01$).

Finally, SpyCatcher003-Dectin-1-sfGFP was used to stain living yeast cells. After staining for 60 min, the sfGFP fluorescence signal was observed accumulating at the perimeter of yeast cells, consistent with cell wall staining (Figure 4). Binding to yeast was reduced by the addition of β-1,3/1,6 glucans. While there was a detectable staining of the entire cell perimeter, a pronounced enrichment of the SpyCatcher003-Dectin-1-sfGFP signal was observed at discrete foci that matched the budding scar enrichment pattern described for other Dectin-1 fusion proteins [20,21]. This confirmed that our SpyCatcher003-Dectin-1-sfGFP retained the ability to bind β-1,3/1,6 glucans present in fungal cell walls and could thus function to target a drug-loaded nanodisc to inhibit yeast proliferation in a liquid culture.

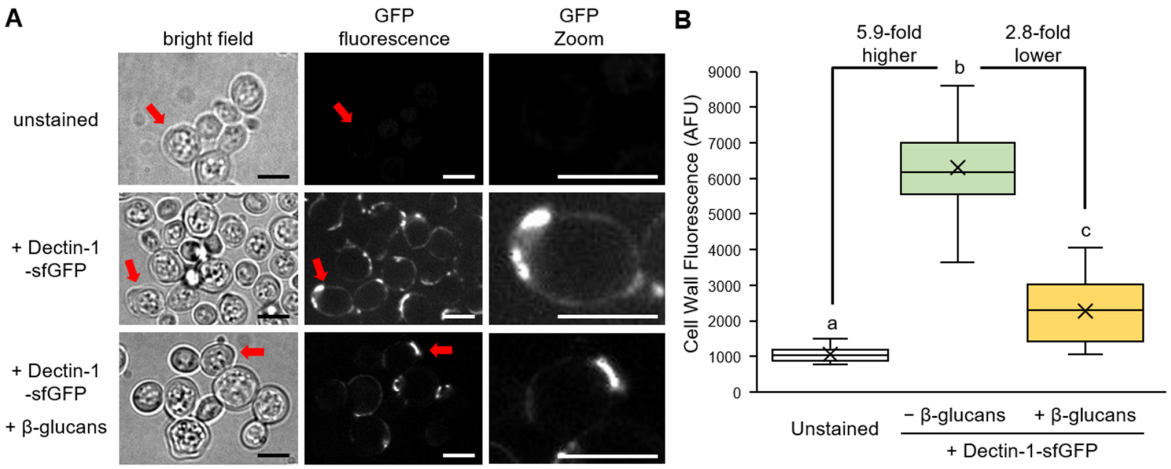


Figure 4. Fluorescence microscopy showing that Dectin-1-sfGFP accumulates at yeast cell walls. (**A**) Confocal fluorescence imaging of yeast cells stained with SpyCatcher003-Dectin-1-sfGFP, with or without a β-1,3/1,6 glucan competitor. Bright field and GFP channel images shown. Red arrows mark the cell highlighted in GFP zoom. Scale bars are 3 µm. (**B**) Quantified GFP channel fluorescence intensity for yeast cell walls. Box represents median and upper/lower quartiles, cross represents mean, whiskers represent range. n = 25 yeast cell perimeters analyzed per condition, observed over three separate staining events. Different letters indicate significant differences from Student's t-tests ($p < 0.00001$).

3. Discussion

The results presented here establish a modular strategy whereby Apolipoprotein-derived lipid nanodiscs are targeted to specific cell types using a SpyCatcher–SpyTag system to covalently couple the nanodisc module to proteins capable of binding unique cellular surface features. The specific example documented here involved coupling Dectin-1 to ApoA1 lipid nanodiscs loaded with the antifungal AmphB, a design intended to target the antifungal-loaded nanodiscs to the β-1,3/1,6 glucans present in the cell walls of most fungi. Nanodiscs themselves have already been shown to enhance the toxicity of AmphB in yeast growth assays [8,9]. Here, we provided a real-time assessment of *S. cerevisiae* growth inhibition when cultures were exposed to either AmphB controls, AmphB-loaded ApoA1 lipid nanodiscs, or Dectin-1-labeled AmphB lipid nanodiscs. In these assays, the Dectin-1 labeling enhanced the toxicity of AmphB, as quantified by an IC_{50} 1.5-fold lower than uncoupled AmphB nanodiscs and 2.8-fold lower than AmphB-only controls (Figure 2). Fluorescence microscopy indicated that the Dectin-1 protein accumulates at the cell wall within an hour (Figure 4), primarily at foci that were previously identified as budding scars [20,21]. Together, these results suggest that Dectin-1-coupled nanodiscs target AmphB to yeast cell walls, resulting in improved antifungal delivery and enhanced toxicity.

A major concern regarding the use of AmphB in human patients is the harmful side-effects of the drug, notably on the kidneys [22]. Pharmaceutical formulations reduce these side-effects by encapsulating the AmphB in liposomes, which allows for the use of higher dosages without increased adverse incidents [23,24]. Like liposomes, lipid nanodiscs themselves have been shown to reduce certain side-effects associated with AmphB [7,9]. We speculate that Dectin-1-labeled AmphB nanodiscs could further reduce side-effects by preferentially targeting AmphB delivery to fungal cells [25]. In both topical and intravenous applications, the Dectin-1 AmphB nanodiscs would be expected to increase the local drug concentration in the proximity of a yeast cell or cell cluster. Future testing will be required to determine whether Dectin-1 AmphB nanodiscs could improve outcomes in patients suffering from fungal infections.

Beyond Dectin-1-mediated targeting benefits, there are additional applications enabled by a modular system in which different SpyCatcher modules can be designed to decorate lipid nanodiscs with a variety of specific ligand-binding proteins. Within the realm of antifungal drug delivery, a consortium of yeast cell wall-binding proteins could be explored for their ability to enhance lipid nanodisc targeting to yeast cells. While Dectin-1 targets primarily β-1,3 and β-1,3/1,6 glucans that are common fungal biopolymers, these are not major surface features in all pathogenic fungi. For example, β-glucans are minimal components of *Cryptococcus* and *Mucorales* cell walls and are absent from *Microsporidia* [26–28]. The emerging antifungal-resistant *Candida auris* strains are also low in β-glucans and use N-linked mannan masking strategies to avoid detection by Dectin-1 [29–31]. Thus, designing additional SpyCatcher003 fusions to proteins that bind α-mannans, chitin, chitosan, or other fungal cell wall components could be harnessed into a modular toolbox for labeling lipid nanodiscs packed with potent antifungal drugs.

Besides targeting fungi, the flexible modular design presented here for ApoA1 nanodiscs could be adapted to target a variety of lipophilic drugs to bacterium, cancer cells, or other desired targets. Recently, a related SpyCatcher strategy was used to generate styrene–maleic acid nanodiscs with an affibody targeting Epidermal Growth Factor receptors in mammalian cells, which was used to preferentially deliver a chemotherapy drug to cancer cells [32]. In this example, the SpyCatcher present in the styrene-based nanodiscs was isolated from the membranes of a mammalian HEK293 cell line expressing a membrane-tethered SpyCatcher [33]. By contrast, the ApoA1 nanodiscs used here have a SpyTag covalently attached to the C-terminal end of an ApoA1 peptide. This direct attach-

ment of the SpyTag to the nanodisc-forming ApoA1 module provides flexibility to allow nanodiscs to be easily generated with a choice of specific membrane lipids and cargoes.

4. Materials and Methods

4.1. Molecular Cloning

Plasmid DNA for 6xHis-ApoA1-SpyTag003 (plasmid stock ps3878) was obtained from previously published sources [34]. 6xHis-SpyCatcher003-sfGFP (ps3702) was obtained from Addgene (133449). An *E. coli* codon-optimized extracellular receptor domain of mouse Dectin-1(69–244) was synthesized (IDT, Coralville, IA, USA) (ps3555). 6xHis-SpyCatcher003-sfGFP was linearized with BamHI (NEB, Ipswich, MA, USA), and a PCR-derived Dectin-1 fragment was added using 2× Hifi Assembly (NEB, Ipswich, MA, USA) to make 6xHis-SpyCatcher003-Dectin-1-sfGFP (ps3784). Sequences were confirmed through whole-plasmid sequencing. See Supplemental Figure S4 for full plasmid sequences.

4.2. E. coli Growth and Protein Expression

Plasmid DNA was transformed into *E. coli* NiCo21 DE3 cells (NEB, Ipswich, MA, USA) and selected on 2xYT agar plates supplemented with antibiotics. 6xHis-ApoA1-SpyTag003 was selected on kanamycin (50 mg/L) and 6xHis-SpyCatcher003-Dectin-1-sfGFP on ampicillin (200 mg/L). Plate growth occurred overnight at 37 °C. Single colonies were used to inoculate 1 mL cultures of 2xYT liquid media and were grown overnight at 37 °C with shaking. Cells were then used to inoculate 200 mL 2xYT cultures, which were grown at 37 °C with shaking until OD600 = 0.6–0.8. Protein expression was induced by adding 0.5 mM isopropyl-(β)-D-1-thiogalactopyranoside and 3% ethanol (v/v). 6xHis-ApoA1-SpyTag003 induction occurred for 4 h at 30 °C with shaking. 6xHis-SpyCatcher003-Dectin-1-sfGFP induction occurred overnight at 18 °C with shaking.

Cells were chilled on ice for 30 min and then pelleted through centrifugation at 6000× g and 4 °C for 15 min. Bacterial pellets were resuspended in lysis buffers supplemented with 1 mg/mL egg lysozyme and 1 mM phenylmethylsulfonyl fluoride (PMSF). Lysis buffer for the 6xHis-ApoA1-SpyTag003 purifications contained 20 mM Tris, 500 mM NaCl, and 10% glycerol (v/v), with a pH 8 at 4 °C. Lysis buffer for the 6xHis-SpyCatcher003-Dectin-1-sfGFP purifications contained 6 M guanidine HCl, 100 mM Na_2HPO_4:NaH_2PO_4 (1:9), 100 mM NaCl, 10 mM triethanolamine, 5 mM β-mercaptoethanol (BME), and 0.1% Triton X-100 (v/v), pH 8 at 4 °C, in accordance with the established Dectin-1 purification techniques [19]. Samples were frozen at −20 °C overnight prior to further purification steps.

4.3. Protein Purification

Frozen bacterial samples were thawed in a hot water bath, and fresh PMSF was added. 6xHis-ApoA1-SpyTag003 samples had Triton X-100 added to 0.4% (v/v) after thawing. Lysis was completed and viscosity was reduced through sonication using a Branson Sonifier 450 (Branson Ultrasonics, Brookfield, CT, USA), 30% duty cycle, output 3. Samples were centrifuged at 12,000× g at 4 °C for 30 min to pellet insoluble elements. The soluble supernatant fractions were added to Ni-NTA beads to bind 6xHis-tagged proteins for 1 h at 4 °C on a nutating mixer.

For 6xHis-ApoA1-SpyTag003 samples, beads were washed in 6xHis wash buffer (20 mM Tris, 100 mM NaCl, 10 mM imidazole, pH 8 at 4 °C) and then eluted in the same buffer containing 300 mM imidazole. Chitin magnetic beads (NEB, Ipswich, MA, USA) were used to remove common 6xHis contaminants according to NiCo21 DE3 strain guidelines. For 6xHis-SpyCatcher003-Dectin-1-sfGFP, beads were first washed with denaturing wash buffer (6 M guanidine HCl, 100 mM Na_2HPO_4:NaH_2PO_4 (1:9), 100 mM NaCl, 10 mM triethanolamine, 5 mM BME, 0.1% Triton X-100 (v/v), 10 mM imidazole, pH 8 at 4 °C).

Subsequent washes were performed with standard 6xHis wash buffer to remove guanidine HCl buffer components, and protein was eluted in standard 6xHis elution buffer. Proteins were concentrated through centrifugation with Pierce Concentrator 10 kDa molecular weight cut-off filters (Thermo Fisher Scientific, Waltham, MA, USA), and glycerol was added to 50% (v/v) before storage at −20 °C.

4.4. Nanodisc Formation and Dectin-1 Labeling

Nanodiscs were prepared as previously described [35]. Briefly, 5 mg of dimyristoyl phosphatidylcholine dissolved in 400 µL of 3:1 chloroform/methanol was added to a 13 × 100 mm borosilicate glass tube and dried under a N_2 (g) stream. To this was added 450 µL of phosphate-buffered saline (PBS), 1 mg of AmphB dissolved in 50 µL of dimethyl sulfoxide (DMSO), and 2 mg of ApoA1-SpyTag003 protein in 6xHis elution buffer, balanced to 1 mL final volume with PBS. External sonication was applied to the glass tube at 27 °C for 10 min to drive nanodisc formation using a water bath sonifier. Nanodisc formation was considered complete when the turbid solution clarified. Samples were centrifuged at 11,000× g at 25 °C for 10 min to pellet and remove any solids that did not incorporate into soluble nanodiscs. The nanodiscs were split into uncoupled controls (i.e., AmphB NDs) and a second fraction to be labeled with Dectin-1 (i.e., Dectin-1 AmphB NDs). Dectin-1 labeling was performed by incubating half the AmphB nanodiscs with 2.7 mg of SpyCatcher003-Dectin-1-sfGFP (1.5:1 molar ratio Dectin-1:ApoA1) for 1 h at 4 °C on a nutating mixer. Conjugation efficiency was analyzed through an analysis of gel bands in Fiji [36], which measures pixel density for each band to calculate abundance ratios.

4.5. Protein Quantification, Gel Analysis, and AmphB Measurements

Protein concentrations were quantified using Bio-Rad protein assay dye reagent (Bio-Rad, Hercules, CA, USA). For gel analysis, 2 µg of protein was mixed with 2× Laemmli loading dye containing 5% BME (v/v) and incubated at 55 °C for 30 min. Samples were analyzed through SDS-PAGE using Mini-Protean TGX precast gels (Bio-Rad, Hercules, CA, USA) run at 175 V for 30 min. Gels were stained with GelCode Blue Safe protein stain (Thermo Fisher Scientific, Waltham, MA, USA), destained in deionized water, and imaged on a Gel Doc XR+ with Image Lab Software v6.1 (Bio-Rad, Hercules, CA, USA).

AmphB content in the nanodiscs and DMSO-solubilized AmphB controls were measured through absorbance spectroscopy at 416 nm using a SmartSpec Plus spectrophotometer (Bio-Rad, Hercules, CA, USA). Samples were dissolved in DMSO for analysis. Total AmphB content was calculated using Beer's law.

4.6. Nanodisc Size Distribution Measurements

Nanodisc size distribution was analyzed through dynamic light scattering using a NICOMP 380 ZLS particle sizer (Particle Sizing Systems, Santa Barbara, CA, USA) equipped with a 12 mW red-laser diode. Samples were diluted in PBS, and the neutral density filter was adjusted to allow for enough counts in the detector. Measurements occurred at 25 °C, with a scattering angle of 90°. Particle distribution was analyzed with Particle Sizing Systems software ZPW 388 Application: version 2.14.0603, and the data was checked against Gaussian and Nicomp distributions.

4.7. Yeast Growth Assays

S. cerevisiae strain W303-1A (*MATa can1 leu2 his3 ade2 trp1 ura3*) [37] (yeast stock ys211) was grown in Synthetic Complete (SC) yeast growth media at 30 °C with shaking for 48 h. Yeast cultures were diluted 500-fold in fresh SC media for use in microtiter assays. Dilutions of AmphB control, Dectin-1-sfGFP control, AmphB nanodiscs, and Dectin-1-labeled AmphB nanodiscs were made in PBS. Each microtiter well received 190 µL yeast-containing SC

media and 10 µL of treatment. Microtiter plates were then used for growth analysis in a Bioscreen C (OY Growth Curves, Helsinki, Finland) with continuous shaking at 30 °C. Absorbance at OD600 was measured for each sample every 10 min. Growth curves were analyzed for log-phase slope changes to determine % inhibition and calculate IC_{50} using Excel (Microsoft, Redmond, WA, USA).

4.8. Yeast Staining and Confocal Fluorescent Microscopy

S. cerevisiae derived from a salt-sensitive G19 strain (*MATa can1 leu2 his3 ade2 trp1 ura3 ena1Δ::HIS3::ena4 Δ*) [38] was grown in liquid SC media at 30 °C with shaking for 48 h. The derivative strain used here (ys289) had been further isolated by the Harper lab as a stable variant that eliminated the presence of polymerized aminoimidazole ribotide, a red pigment with autofluorescence properties that often occurs in *ade*$^{-}$ yeast strains. Yeast cells were pelleted through centrifugation at 21,000× *g* for 2 min, and the media was exchanged with fresh SC supplemented with SpyCatcher003-Dectin-1-sfGFP. For competitor studies, Dectin-1-sfGFP stain media was pre-treated with 25 mg/mL β-1,3/1,6 glucans for 10 min at 30 °C with shaking. Yeast cells were stained in the dark at 30 °C with shaking for 60 min. Cells were re-pelleted through centrifugation, and the stain media was exchanged with fresh SC media. Cell suspensions were pipetted onto a pad of 1.5% agarose (*w*/*v*) in PBS that thinly coated a microscope slide. Samples were partly dried under sterile laminar air flow before adding a cover slip.

Images were captured on a DMi8 inverted microscope (Leica, Wetzlar, Germany) equipped with a CSU-W1 spinning disk confocal scanner module (Yokogawa, Tokyo, Japan) and an Andor iXon Life 888 EMCCD camera (Andor, Belfast, Northern Ireland). The microscope system was operated using VisiView software v6 (Visitron Systems, Puchheim, Germany). Magnification involved a 63×/1.4–0.6 Oil HC PL APO objective (Leica, Wetzlar, Germany) and a 1.6× objective magnifier, yielding a total magnification of 100.8×. Bright-field transmitted light lamp stimulation was 50 au, and images were taken with an exposure time of 150 ms, binning 2, and gain 100. sfGFP was stimulated with a 488 nm single mode diode laser (Toptica, Graefelfing, Germany) at 150 mW (75%). GFP emission was narrowed using an Em 525/50 nm bandpass filter (Chroma, Bellows Falls, VT, USA). GFP images were taken with an exposure time of 400 ms, binning 2, and gain 600. GFP images were set to a fixed 1000–20,000-pixel range using Fiji [36]. GFP signal quantification involved perimeter tracing of the fluorescent signal using Fiji to provide an average intensity value for a yeast cell.

5. Conclusions

The technology developed here uses the SpyCatcher–SpyTag system to allow for a flexible modular labeling of protein–lipid nanodiscs, which has potential for targeting lipophilic drugs to specific cellular targets. Specifically, a receptor that binds fungal cell wall carbohydrates named Dectin-1 was coupled to ApoA1 lipid nanodiscs loaded with the antifungal AmphB, which resulted in an improved inhibition of yeast growth as measured by 1.5-fold lower IC_{50} values. ApoA1 lipid nanodiscs and Dectin-1-sfGFP themselves did not show significant toxicity towards yeast, indicating that the observed effects were dependent on the encapsulation of the AmphB antifungal and its preferential targeting to yeast cells. Obvious extensions of this technology include pairing nanodiscs loaded with different cargoes with different targeting modules (e.g., chemotherapy drugs paired with cancer-targeting proteins, etc.). Regardless, the research presented here establishes an example in which ApoA1 lipid nanodiscs loaded with AmphB can be labeled with Dectin-1-sfGFP using SpyCatcher–SpyTag technology and shows that this Dectin-1 coupling improved AmphB toxicity to yeast.

Supplementary Materials: The following supporting information can be downloaded at: https://www.mdpi.com/article/10.3390/synbio4020007/s1.

Author Contributions: J.A.D. and J.B.T. performed all molecular cloning, protein purification, and yeast growth assays. E.B. and G.B. performed microscopy experiments with assistance from J.A.D., L.C.-E. and M.A.A.-A. performed nanodisc size measurements. J.F.H. supervised all experiments and agrees to serve as author responsible for contact. All authors have read and agreed to the published version of the manuscript.

Funding: Research was funded by the National Science Foundation (IOS-1947741, IOS-2129234, IOS-2450928 to JFH; and CHE-2108462 to MAA-A). JBT received stipend support from a Nevada Undergraduate Research Award.

Institutional Review Board Statement: Not applicable.

Informed Consent Statement: Not applicable.

Data Availability Statement: The original contributions presented in this study are included in the article/Supplementary Materials. Further inquiries can be directed to the corresponding author.

Acknowledgments: Thanks to the Ryan lab for providing 6xHis-ApoA1-SpyTag003 plasmid and guidance on nanodisc formation.

Conflicts of Interest: The authors declare no conflicts of interest.

Abbreviations

The following abbreviations are used in this manuscript:

AmphB	Amphotericin B
ApoA1	Apolipoprotein A-1
SpyC-SpyT	SpyCatcher–SpyTag
ND	Nanodisc
sfGFP	Super Folder Green Fluorescent Protein
PBS	Phosphate-Buffered Saline
BME	β-Mercaptoethanol
DMSO	Dimethyl Sulfoxide
PMSF	Phenylmethylsulfonyl Fluoride
SC	Synthetic Complete

References

1. Dong, Y.; Tang, H.; Dai, H.; Zhao, H.; Wang, J. The application of nanodiscs in membrane protein drug discovery & development and drug delivery. *Front. Chem.* **2024**, *12*, 1444801. [CrossRef]
2. Denisov, I.G.; Sligar, S.G. Nanodiscs in Membrane Biochemistry and Biophysics. *Chem. Rev.* **2017**, *117*, 4669–4713. [CrossRef] [PubMed]
3. Bayburt, T.H.; Grinkova, Y.V.; Sligar, S.G. Self-Assembly of Discoidal Phospholipid Bilayer Nanoparticles with Membrane Scaffold Proteins. *Nano Lett.* **2002**, *2*, 853–856. [CrossRef]
4. Raussens, V.; Narayanaswami, V.; Goormaghtigh, E.; Ryan, R.O.; Ruysschaert, J.M. Alignment of the apolipophorin-III alpha-helices in complex with dimyristoylphosphatidylcholine. A unique spatial orientation. *J. Biol. Chem.* **1995**, *270*, 12542–12547. [CrossRef] [PubMed]
5. Tall, A.R.; Small, D.M. Solubilisation of phospholipid membranes by human plasma high density lipoproteins. *Nature* **1977**, *265*, 163–164. [CrossRef]
6. Benedicto, V.G.L.; Haguar, Z.; Abdulhasan, A.; Narayanaswami, V. Apolipoprotein E3 Containing Nanodiscs as Vehicles for Transport and Targeted Delivery of Flavonoid Luteolin. *ACS Omega* **2024**, *9*, 2988–2999. [CrossRef]
7. Tufteland, M.; Ren, G.; Ryan, R.O. Nanodisks derived from amphotericin B lipid complex. *J. Pharm. Sci.* **2008**, *97*, 4425–4432. [CrossRef]
8. Oda, M.N.; Hargreaves, P.L.; Beckstead, J.A.; Redmond, K.A.; van Antwerpen, R.; Ryan, R.O. Reconstituted high density lipoprotein enriched with the polyene antibiotic amphotericin B. *J. Lipid Res.* **2006**, *47*, 260–267. Correction in *J. Lipid Res.* **2006**, *47*, 1114. https://doi.org/10.1194/jlr.D500033-JLR200. [CrossRef]

9. Burgess, B.L.; He, Y.; Baker, M.M.; Luo, B.; Carroll, S.F.; Forte, T.M.; Oda, M.N. NanoDisk containing super aggregated amphotericin B: A high therapeutic index antifungal formulation with enhanced potency. *Int. J. Nanomed.* **2013**, *8*, 4733–4742. [CrossRef]
10. Pérez-de-Luque, A.; Cifuentes, Z.; Beckstead, J.A.; Sillero, J.C.; Ávila, C.; Rubio, J.; Ryan, R.O. Effect of amphotericin B nanodisks on plant fungal diseases. *Pest Manag. Sci.* **2012**, *68*, 67–74. [CrossRef]
11. Zakeri, B.; Fierer, J.O.; Celik, E.; Chittock, E.C.; Schwarz-Linek, U.; Moy, V.T.; Howarth, M. Peptide tag forming a rapid covalent bond to a protein, through engineering a bacterial adhesin. *Proc. Natl. Acad. Sci. USA* **2012**, *109*, E690–7. [CrossRef]
12. Keeble, A.H.; Turkki, P.; Stokes, S.; Anuar, I.N.A.K.; Rahikainen, R.; Hytönen, V.P.; Howarth, M. Approaching infinite affinity through engineering of peptide-protein interaction. *Proc. Natl. Acad. Sci. USA* **2019**, *116*, 26523–26533. [CrossRef] [PubMed]
13. Brown, G.D.; Gordon, S. Immune recognition. A new receptor for beta-glucans. *Nature* **2001**, *413*, 36–37. [CrossRef] [PubMed]
14. Brown, G.D.; Taylor, P.R.; Reid, D.M.; Willment, J.A.; Williams, D.L.; Martinez-Pomares, L.; Wong, S.Y.; Gordon, S. Dectin-1 Is A Major β-Glucan Receptor On Macrophages. *J. Exp. Med.* **2002**, *196*, 407. [CrossRef] [PubMed]
15. Gringhuis, S.I.; Den Dunnen, J.; Litjens, M.; Van Der Vlist, M.; Wevers, B.; Bruijns, S.C.; Geijtenbeek, T.B. Dectin-1 directs T helper cell differentiation by controlling noncanonical NF-kappaB activation through Raf-1 and Syk. *Nat. Immunol.* **2009**, *10*, 203–213. [CrossRef]
16. Gross, O.; Gewies, A.; Finger, K.; Schäfer, M.; Sparwasser, T.; Peschel, C.; Förster, I.; Ruland, J. Card9 controls a non-TLR signalling pathway for innate anti-fungal immunity. *Nature* **2006**, *442*, 651–656. [CrossRef]
17. Underhill, D.M.; Rossnagle, E.; Lowell, C.A.; Simmons, R.M. Dectin-1 activates Syk tyrosine kinase in a dynamic subset of macrophages for reactive oxygen production. *Blood* **2005**, *106*, 2543–2550. [CrossRef]
18. Gantner, B.N.; Simmons, R.M.; Canavera, S.J.; Akira, S.; Underhill, D.M. Collaborative Induction of Inflammatory Responses by Dectin-1 and Toll-like Receptor 2. *J. Exp. Med.* **2003**, *197*, 1107. [CrossRef]
19. Ambati, S.; Ferarro, A.R.; Khang, S.E.; Lin, J.; Lin, X.; Momany, M.; Lewis, Z.A.; Meagher, R.B. Dectin-1-Targeted Antifungal Liposomes Exhibit Enhanced Efficacy. *mSphere* **2019**, *4*, e00025-19. Erratum in: *mSphere* **2019**, *4*, e00121-19. https://doi.org/10.1128/MSPHERE.00025-19. [CrossRef]
20. de Assis, L.J.; Bain, J.M.; Liddle, C.; Leaves, I.; Hacker, C.; da Silva, R.P.; Yuecel, R.; Bebes, A.; Stead, D.; Childers, D.S.; et al. Nature of b-1,3-Glucan-Exposing Features on Candida albicans Cell Wall and Their Modulation. *mBio* **2022**, *13*, e02605-22. [CrossRef]
21. Gantner, B.N.; Simmons, R.M.; Underhill, D.M. Dectin-1 mediates macrophage recognition of Candida albicans yeast but not filaments. *EMBO J.* **2005**, *24*, 1277–1286. [CrossRef] [PubMed]
22. Cavassin, F.B.; Baú-Carneiro, J.L.; Vilas-Boas, R.R.; Queiroz-Telles, F. Sixty years of Amphotericin B: An Overview of the Main Antifungal Agent Used to Treat Invasive Fungal Infections. *Infect. Dis. Ther.* **2021**, *10*, 115–147. [CrossRef] [PubMed]
23. Nokura, Y.; Maezawa, M.; Miyasaka, K.; Hirofuji, S.; Nakao, S.; Yamashita, M.; Ichihara, N.; Sugishita, K.; Tamaki, H.; Iguchi, K.; et al. Comparison of Adverse Event Profiles of Amphotericin B Formulations Using Real-World Data. *Cureus* **2024**, *16*, e71588. [CrossRef] [PubMed]
24. Stone, N.R.H.; Bicanic, T.; Salim, R.; Hope, W. Liposomal Amphotericin B (AmBisome®): A Review of the Pharmacokinetics, Pharmacodynamics, Clinical Experience and Future Directions. *Drugs* **2016**, *76*, 485–500. [CrossRef]
25. Sousa, F.; Ferreira, D.; Reis, S.; Costa, P. Current Insights on Antifungal Therapy: Novel Nanotechnology Approaches for Drug Delivery Systems and New Drugs from Natural Sources. *Pharmaceuticals* **2020**, *13*, 248. [CrossRef]
26. Ruiz-Herrera, J.; Ortiz-Castellanos, L. Cell wall glucans of fungi. A review. *Cell Surf.* **2019**, *5*, 100022. [CrossRef]
27. Cheng, Q.; Widanage, M.C.D.; Yarava, J.R.; Ankur, A.; Latgé, J.-P.; Wang, P.; Wang, T. Molecular architecture of chitin and chitosan-dominated cell walls in zygomycetous fungal pathogens by solid-state NMR. *Nat. Commun.* **2024**, *15*, 8295. [CrossRef]
28. Theel, E.S.; Doern, C.D. β-d-Glucan Testing Is Important for Diagnosis of Invasive Fungal Infections. *J. Clin. Microbiol.* **2013**, *51*, 3478. [CrossRef]
29. Farooqi, J.; Niamatullah, H.; Irfan, S.; Zafar, A.; Malik, F.; Jabeen, K. Comparison of β-D-Glucan levels between Candida auris and other Candida species at the time of candidaemia: A retrospective study. *Clin. Microbiol. Infect.* **2021**, *27*, 1519.e1–1519.e5. [CrossRef]
30. Wang, Y.; Zou, Y.; Chen, X.; Li, H.; Yin, Z.; Zhang, B.; Xu, Y.; Zhang, Y.; Zhang, R.; Huang, X.; et al. Innate immune responses against the fungal pathogen Candida auris. *Nat. Commun.* **2022**, *13*, 3553. [CrossRef]
31. Horton, M.V.; Eix, E.F.; Johnson, C.J.; Dean, M.E.; Andes, B.D.; Wartman, K.M.; Nett, J.E. Impact of Micafungin on Candida auris β-glucan Masking and Neutrophil Interactions. *J. Infect. Dis.* **2024**, *230*, 763–767. [CrossRef]
32. Noh, I.; Guo, Z.; Wang, R.; Zhu, A.T.; Krishnan, N.; Mohapatra, A.; Gao, W.; Fang, R.H.; Zhang, L. Modular functionalization of cellular nanodiscs enables targeted delivery of chemotherapeutics into tumors. *J. Control. Release* **2025**, *378*, 145–152. [CrossRef]
33. Krishnan, N.; Jiang, Y.; Zhou, J.; Mohapatra, A.; Peng, F.-X.; Duan, Y.; Holay, M.; Chekuri, S.; Guo, Z.; Gao, W.; et al. A modular approach to enhancing cell membrane-coated nanoparticle functionality using genetic engineering. *Nat. Nanotechnol.* **2023**, *19*, 345–353. [CrossRef]
34. Veron, B.S.; Lethcoe, K.; Ryan, R.O. Immobilized nanodisks for study of ligand binding interactions. *Biochim. Biophys. Acta BBA Biomembr.* **2025**, *1867*, 184459. [CrossRef]

35. Lethcoe, K.; Fox, C.A.; Moh, I.; Swackhamer, M.; Karo, M.; Lockhart, R.; Ryan, R.O. Formulation and Characterization of Bioactive Agent Containing Nanodisks. *J. Vis. Exp.* **2023**, *193*, e65145. [CrossRef]
36. Schindelin, J.; Arganda-Carreras, I.; Frise, E.; Kaynig, V.; Longair, M.; Pietzsch, T.; Preibisch, S.; Rueden, C.; Saalfeld, S.; Schmid, B.; et al. Fiji: An open-source platform for biological-image analysis. *Nat. Methods* **2012**, *9*, 676–682. [CrossRef]
37. Cunningham, K.W.; Fink, G.R. Calcineurin-dependent growth control in *Saccharomyces cerevisiae* mutants lacking PMC1, a homolog of plasma membrane Ca^{2+} ATPases. *J. Cell Biol.* **1994**, *124*, 351–363. [CrossRef] [PubMed]
38. Quintero, F.J.; Garciadeblás, B.; Rodríguez-Navarro, A. The SAL1 gene of Arabidopsis, encoding an enzyme with 3′(2′),5′-bisphosphate nucleotidase and inositol polyphosphate 1-phosphatase activities, increases salt tolerance in yeast. *Plant Cell* **1996**, *8*, 529–537. [CrossRef] [PubMed]

Disclaimer/Publisher's Note: The statements, opinions and data contained in all publications are solely those of the individual author(s) and contributor(s) and not of MDPI and/or the editor(s). MDPI and/or the editor(s) disclaim responsibility for any injury to people or property resulting from any ideas, methods, instructions or products referred to in the content.